Hindawi
Scientific Programming
Volume 2022, Article ID 7702776, 8 pages
https://doi.org/10.1155/2022/7702776

Research Article

Preparation of Nitrogen-Doped Carbon-Based Bimetallic Copper-Cobalt Catalysis Based on Deep Learning and Its Monitoring Application in Furfural Hydrogenation

Xiaojun Pei, Haojun Shu, and Yisi Feng

School of Chemistry and Chemical Engineering, Hefei University of Technology, Hefei 230009, China

Correspondence should be addressed to Yisi Feng; fengyisi@hfut.edu.cn

Received 6 April 2022; Revised 14 April 2022; Accepted 25 April 2022; Published 20 May 2022

Academic Editor: Jie Liu

In the field of catalysis, the support of the catalyst is often composed of hollow carbon materials. In order to monitor the preparation of nitrogen-doped carbon-based bimetallic copper-cobalt catalysis and its hydrogenation reaction in furfural, using m-aminophenol as the nitrogen source, formaldehyde as a carbon source, and P123 as a template agent, a nitrogen-doped bimetallic copper-cobalt mesoporous carbon catalyst Cu-Co@N-MPC-500 was synthesized by the hydrothermal method. The morphology, structure, and chemical composition of the catalyst were analyzed by means of TEM, XRD, BET, and XPS, respectively. The results show that the nitrogen-doped mesoporous carbon has a stable structure, uniform pore size distribution, and the nano-copper-cobalt particles are uniformly dispersed in the mesoporous carbon surface. Through furfural hydrogenation, the catalyst selectivity and cycle stability were discussed. Under the furfural conversion rate of 96.1%, the yield of cyclopentanone could reach 76.2%. After 5 cycles, the catalytic efficiency of the catalyst did not decrease significantly. It shows that Cu-Co@N-MPC-500 has excellent application prospects in the field of industrial production.

1. Related Introduction

Porous carbon materials come from a wide range of sources, including mesoporous carbon, activated carbon, carbon nanotubes, graphene, amorphous carbon black, nanofibers, and carbon aerogels. Porous carbon materials are widely used in catalysis, adsorption electrochemical [1–3], and other important fields. However, pure carbon porous materials do not perform well in many applications, and carbon materials need to be further modified to improve their application performance.

In the field of catalysis, porous carbon materials are often used as catalyst supports. Introducing other atoms into the carbon atomic layer to modify porous carbon materials to improve the reactivity of catalysts has been a research hotspot in recent years. The introduction of sulfonic acid groups into the porous carbon support can effectively introduce acid sites into the catalyst, thereby changing the acid value of the catalytic material. Kasakov et al. used glucose and cellulose as porous carbon sources to prepare a sulfonic acid group-modified Ni/C-SO3H catalyst, which showed excellent catalytic activity in the liquid-phase hydrogenation of phenol to cyclohexane. After reacting at 200°C for 6 h, the conversion of phenol and the yield of cyclohexane can reach 100% and 90%, respectively. Onda et al. [4, 5] used activated carbon (AC) as the carbon source to prepare a sulfonic acid group-modified platinum catalyst Pt/AC-SO_3H by modifying the carbon material. The activity of the catalyst was tested in the reaction of hydrolysis of polysaccharides to gluconic acid; the results show that the catalyst Pt/AC-SO_3H modified by sulfonic acid group has a significantly higher catalytic effect than the traditional carbon-based supported catalyst. N doping is one of the most common carbon-based support modification strategies. N atoms are doped into carbon to make the carbon structure more disordered, which will increase the defect sites of the carbon support and make N-doped carbon materials have unique properties [6]. The use of nitrogen-doped carbon-based supports can effectively improve the hydrophilicity and conductivity of the catalyst, strengthen the interaction between the carbon support and

the metal active components, improve the stability of the catalyst, and at the same time play a role in regulating the supported metal active components [7]. Lei [8] et al. used the hard template method to mix SBA-15 with aniline and then carbonized and removed the template at high temperature to prepare a nitrogen-doped ordered mesoporous carbon-supported metal Pt catalyst, which was investigated in the catalytic oxidation of methanol. The results show that there is a strong interaction between the nitrogen element in the carrier and the metal active component Pt nanoparticles. The higher the doping amount of nitrogen in the carrier, the higher the dispersion degree of Pt metal nanoparticles. Moreover, the prepared catalyst showed good reactivity in methanol oxidation reaction. Chan-Thaw et al. [9] prepared a nitrogen-doped carbon nanotube-supported palladium metal catalyst, which showed better catalytic performance in the catalytic oxidation reaction system of benzyl alcohol than the traditional activated carbon nanotube-supported palladium metal catalyst. There are many application reports on the use of modified carbon materials as catalyst supports to support single metals, but there are few reports on the use of modified carbon materials to support nonprecious bimetallic components.

The related research study in this paper is mainly based on using $Cu(NO_3)_2{\cdot}3H_2O$ and $Co(NO_3)_2{\cdot}6H_2O$ as the precursors of metal active components, by using the triblock compound P 123 as the soft template and m-aminophenol as the nitrogen source, formaldehyde was used as the carbon source, and then a nitrogen-doped carbon-based bimetallic catalyst 2Cu-Co@N-MPC-500 was prepared through a one-step hydrothermal reaction, high-temperature carbonization, and H_2 reduction. The catalyst structure and components were characterized and analyzed, and the performance of the prepared catalyst was examined in the hydrogenation of biomass molecule furfural to cyclopentanone.

2. Related Theoretical Methods

The RNN network is also composed of an input layer, hidden layer, and output layer. Each layer contains a different number of neurons. In the traditional neural network model, the neurons of each layer are not connected to each other, but the RNN network is different, and the nodes between its hidden layers are connected. Therefore, the biggest difference between the RNN neural network and traditional neural network model is that RNN neural network not only has feedforward connection, but also has feedback of internal connection, which plays the role of "circulation." This kind of information flow similar to feedback inside neurons makes the network have memory function. At a certain time *t*, the difference between the neurons of the BP neural network and the neurons of the RNN network is shown in Figure 1:

There are many variants of the RNN network model, among which, Figure 2-1 is expanded in time series, and the classic RNN network model structure is shown in Figure 3:

In the above figure, the meaning of each parameter is as follows:

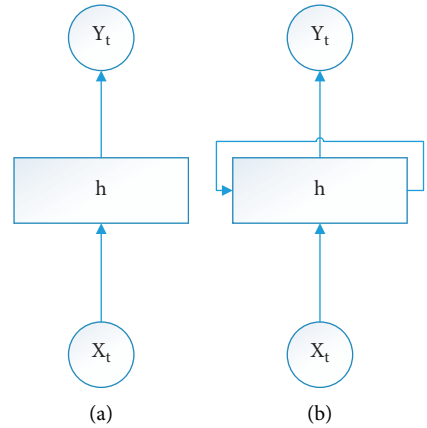

Figure 1: (a)BP neuron and (b) RNN neuron.

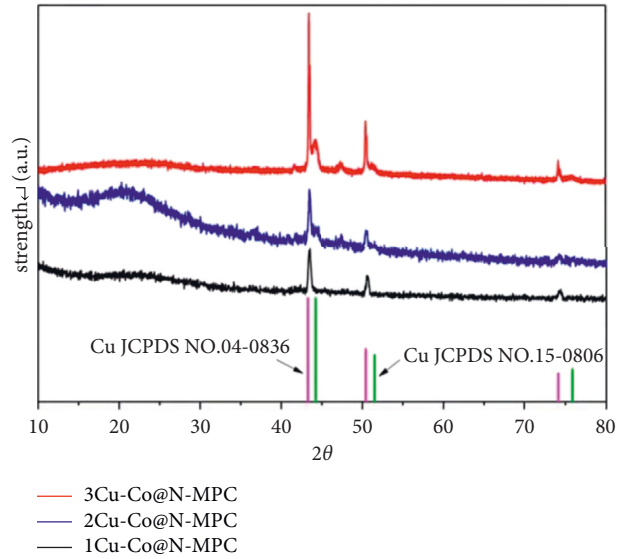

Figure 2: XRD characterization results of different Cu-Co loadings.

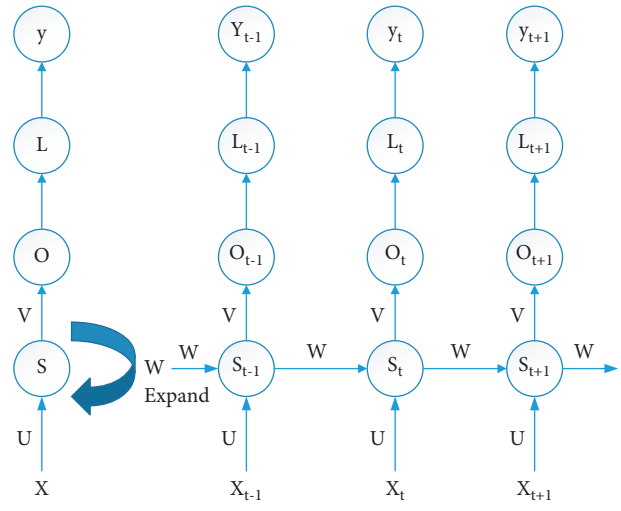

Figure 3: RNN network structure diagram.

(1) U, V, and W are three matrices, which represent the input weight, the output weight, and the last output as the weight of this input, respectively. These three matrices are the linear relationship parameters of the model. The reason why the RNN network can have memory depends on these three matrices.

(2) x represents the input layer data. Also, s_{t-1}, s_t, and s_{t+1} represent the input values at $t-1$, t, and $t+1$, respectively.

(3) s represents the hidden layer state. Similarly, s_t represents the state of the hidden layer at time t. As shown in Figure 2-2, both x_t and st-1 will affect s_t.

(4) o represents the output of the model. As can be seen from the figure, o is only associated with s_t.

(5) L is the loss function of the model.

(6) y is the true observed value of the predicted time series data. As can be seen from Figure 2-2, in the RNN network, the hidden state s_t at any time can be obtained by the following equation:

$$s_t = \sigma(Ux_t + Ws_{t-1} + b). \tag{1}$$

In formula (1) and the following equations, σ is the activation function and b is the bias of the linear relationship.

After obtaining the state s_t of the hidden layer of the model at time t, the model output o_t at this time can be obtained by the following: t to

$$o_t = VS_t + c. \tag{2}$$

In formula (2), c also represents the bias, so the final output predicted by the RNN network can be obtained from the following:

$$\widehat{y}_t = \sigma(o_t). \tag{3}$$

After the predicted output value is obtained, the cost function can be used to quantify the loss of the RNN model at the current time t, that is, the gap between the predicted value $\widehat{y}_t$ of the model and the original real data y_t. Common cost functions include cross-entropy cost function, mean squared error, root mean squared error, etc. This is actually the forward propagation algorithm of the RNN network model. In this paper, the preparation of a nitrogen-doped carbon-based bimetallic copper-cobalt catalyst based on in-depth learning and its monitoring application in furfural hydrogenation are studied. The main reason is that the relevant experimental results are monitored by computer technology.

3. Experimental Part

3.1. Reagents and Equipment. The reagents prepared in the relevant experiments in this paper mainly include "triblock compound P123, (Mn: 2000–5800) obtained from Annaiji; analytical grade m-aminophenol, aqueous formaldehyde solution, and furfural purchased from Sinopharm Chemical Reagent Co. Ltd.; analytical grade copper nitrate trihydrate, cobalt nitrate hexahydrate, anhydrous hexanol, and ethyl acetate obtained from Aladdin."

The main equipment prepared in this paper for related experiments are "superconducting nuclear magnetic resonance spectrometer (VNMRS600), Agilent Technologies, USA; X-ray photoelectron spectrometer (ESCACAB250), Thermo Fisher, USA; X-ray diffractometer (X-ray diffractometer 'Pert PRO MPD type), PANalytical company, Netherlands; scanning electron microscope (SU8020 type), Hitachi, Japan; elemental analyzer (vario EL cube), Germany Elementar company; tube roasting furnace (GSL-1500X type), Hefei Kejing Materials Co., Ltd.; gas adsorption instrument (Autosorb-IQ3 type), American Quanta; and a gas chromatograph (GC16901FJ type), Hefei Jiedao Equipment Co. Ltd."

3.2. Preparation of Catalysts. The preparation of the catalyst is mainly prepared by the hydrothermal method, and its main principle is to carry out the index through the hydrothermal reaction kettle, namely, the preparation of N-doped mesoporous carbon catalysts by the hydrothermal method: 1.01 g $Cu(NO_3)_2{\cdot}3H_2O$ and 0.62 g $Co(NO_3)_2{\cdot}6H_2O$ with a molar ratio of 2 : 1 were dissolved in 50 mL of ethanol and 50 mL of deionized mixed solution of water, 4.5 g of m-aminophenol and 1.0 g of templating agent P123 were sequentially added, and stirred until completely dissolved. Then, 4.5 g formaldehyde solution (37 wt%) was slowly added to the solution using a dropping funnel, and the dropwise addition time was controlled to be 1 h. After the dropwise addition was completed, the reaction was continued at room temperature for 2 h.

The solution was transferred to a hydrothermal reactor, sealed, and placed in a drying oven at 65°C for 5 h. The obtained reaction mixture was filtered with deionized water and ethanol solution, and the filter cake obtained by filtration was dried in a vacuum drying oven at 60°C overnight. The dried solid was taken out and ground into powder using a mortar. The obtained powder was placed in a tube furnace for high-temperature carbonization. The tube furnace was heated from 25°C to 500°C at a heating rate of 1°C/min, and kept at 500°C for 2 hours. The carbonization process was carried out in a mixed atmosphere of nitrogen and hydrogen. A nitrogen-doped ordered mesoporous carbon was obtained, which was denoted as 2Cu-Co@N-MPC-500, where 2 represents the molar ratio of metal Cu and Co and 500 is the calcination temperature.

As a comparison, traditional activated carbon supported catalysts were prepared by the impregnation method. First, 1.01 g $Cu(NO_3)_2$ $3H_2O$ and 0.31 g $Co(NO_3)_2$ $6H_2O$ were added to 90 mL of dilute nitric acid (5 wt%) solution at a temperature of 60°C and stirred rapidly for 2 h, and then it was put into an ultrasonic instrument for ultrasonic treatment for 2 h, 2.3 g of activated carbon was added into the above solution, and mechanical stirring was performed for 2 h; then the above mixture was filtered and washed. The filter cake was transferred to an oven at 60°C for vacuum drying and then ground into powder using a grinder. The obtained powder is placed in a tube furnace for high-

temperature carbonization, and the carbonization conditions are the same as those for preparing the catalyst by the hydrothermal method. An activated carbon-supported catalyst was obtained, which is denoted as 2Cu-Co@AC-500 as shown in Figure 4.

3.3. Characterization of Catalysts. The catalytic materials were analyzed for specific surface area, pore volume, and pore size distribution using a fully automatic surface area analyzer (BET). The specific method is as follows: 0.1 g of the sample was weighed, and after 4 hours of treatment under vacuum conditions, the adsorption and desorption test was carried out in a liquid nitrogen atmosphere. The specific surface area of the material was calculated using the BET (Brunner–Emmet–Teller) formula, and the pore size distribution was calculated using the BJH formula. The bulk structure analysis of nitrogen-doped catalysts was performed using X-ray powder diffraction analysis (XRD). Using Cu-Kα as the X-ray radiation source, the scanning speed is 8°/min; the scanning test angle range is 20°–90°, and the working voltage and current of the instrument are 40 kV and 55 mA, respectively. The metal elements in the catalysts were quantitatively and qualitatively analyzed by X-ray photoelectron spectroscopy (XPS), and the metal grain size was calculated by the Scherrer formula. Using transmission electron microscopy (TEM) to conduct microscopic analysis of the apparent morphology and structure of the catalytic materials, qualitative and semiquantitative analysis of the composition of the catalytic materials can also be carried out. Before testing, the samples were ground to powder, and then dispersed evenly in ethanol solution, sonicated for 1 h with an ultrasonic instrument, and then the suspension was evenly spread on the copper mesh for testing. The metal content components in the catalysts were detected by an -inductively coupled plasma analyzer (ICP-AES). Before detection, concentrated nitric acid was used to dissolve a certain amount of the sample catalyst, and then diluted to constant volume for sample detection.

3.4. Performance Test of Catalysts. In the furfural hydrogenation reaction, it needs to be carried out in a batch autoclave, and the activity of nitrogen-doped mesoporous carbon-supported metal copper-cobalt catalysts is prepared by a temperature controller and a 25 mL batch autoclave with magnetic stirring.

The experimental operation is as follows: accurately weigh 0.2 g of furfural and 0.1 g of the prepared catalyst, add them into the autoclave, then add 10 mL of deionized water, put in the magnet, seal the autoclave, and pass 1.0 MPa hydrogen gas, replace the gas 5 times, then add the hydrogen pressure required for the reaction, heat to the temperature required for the reaction under magnetic stirring at 700 rpm/min, and adjust the heating program and the reaction time by a temperature controller. After the reaction, the mixed solution was transferred to 10 mL of ethyl acetate solution containing quantitative internal standard DMF, and then the reaction solution was filtered, and the filtrate obtained after filtration was detected and analyzed by gas chromatography.

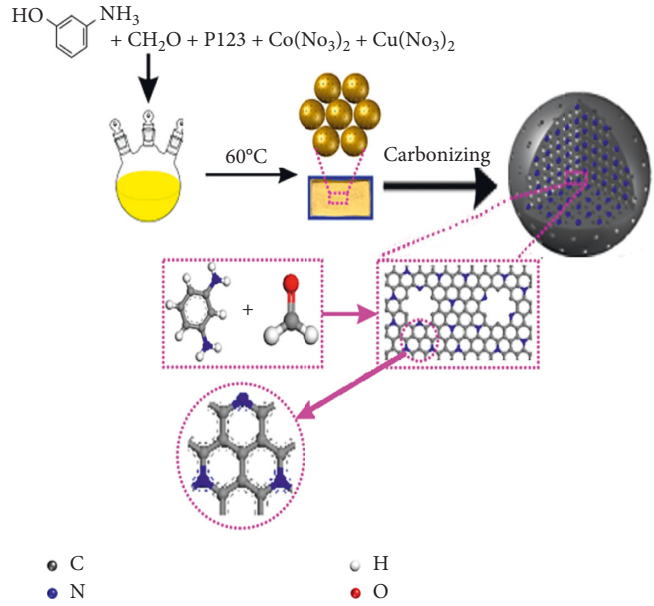

Figure 4: Preparation process of the N-doped mesoporous carbon catalyst.

The furfural hydrogenation reaction products were analyzed by gas chromatography. After the reaction, furfural, furfuryl alcohol, cyclopentanol, cyclopentanone, and tetrahydrofurfuryl alcohol mainly exist in the solution. The detection conditions of the gas chromatograph are as follows: FID detector; chromatographic column; DM-Wax capillary column; detection chamber temperature: 280°C; vaporization chamber temperature: 260°C; carrier gas pressure: 0.1 MPa; column oven initial temperature: 50°C; standard substance: DMF; and sample injection volume: 0.1–0.2 μL.

3.5. Cyclic Performance Test of Catalysts. After each test reaction, the reaction solution was filtered and washed, and the obtained solid filter residue was washed with deionized water and ethanol solution for many times and then sealed and dried in an oven for continued use in the next cycle. In the next cycle experiment, the same mass of the recovered catalyst was weighed as in the last experiment, and control other reaction conditions are set to be the same as the last time.

4. Results and Discussion

4.1. Catalyst Characterization Analysis

4.1.1. XRD Analysis. It can be seen from Figure 2 that the as-prepared Cu-Co@N-MPC exhibits strong diffraction peaks around 43.4° and 50.5°, corresponding to the diffraction peaks of elemental Cu (JCPDS 96-901-2955) [10]. By comparing the peak intensities of catalysts with different Cu loadings, it is found that with the increase of Cu loading, the diffraction peaks of Cu are also continuously enhanced. The diffraction peak observed at about 2θ of 44.8° corresponds to

the diffraction peak of Co, but the peak intensity is weak, which may be due to the good dispersion and small particle size of Co metal nanoparticles. In order to further determine the existence form and valence state of each element in the catalyst, the catalyst was further characterized by XPS.

4.1.2. XPS Analysis. Figure 5 shows the XPS spectrum of 2Cu-Co@N-MPC-500. It can be seen from Figure 4(a) that strong peak signals mainly appear at the binding energies of 932.5 eV and 934.6 eV. The peak at 934.6 eV is the characteristic peak of Cu^{2+}, while the peak at 932.5 eV is the characteristic peak of Cu^{+} and Cu^{0} [11], and the area ratios of Cu^{0} and Cu_2O to CuO are 82.3% and 17.7%, indicating that the Cu-Co@N-Cu in MPC mainly exists in the state of Cu^{0} and Cu_2O, and the reduction of metal Cu is relatively sufficient. The XPS spectrum of Co in 2Cu-Co@N-MPC is shown in Figure 4(d), the binding energy peaks of Co mainly appear at 778.0 eV corresponding to the characteristic peak of Co^{0} (2p 3/2), 780.9 eV and 797.6 eV, respectively. For the characteristic peaks of Co^{3+} (2p 3/2) and Co^{3+} (2p 1/2), 783.5 eV and 796.5 eV correspond to the characteristic peaks of Co^{2+} (2p 3/2) and Co^{2+} (2p 1/2), respectively, indicating that the main forms of copper are CoO and Co_3O_4, and cobalt is less reduced. The metal grain size was calculated to be 13.8 nm by the Scherrer formula. XPS analysis results showed that the metal active centers of the prepared catalysts were mainly Cu^{0}, Cu_2O, and CoO_x.

Figure 5(c) is the XPS characterization spectrum of 2Cu-Co@N-MPC-500N. It can be seen from the figure that the peak of the N1s binding energy in Cu-Co@N-MPC-500 appears at 400.9 eV, which corresponds to graphite nitrogen bonding.

The peak at 398.9 eV corresponds to the binding energy of pyridine nitrogen. The ratio of graphitic nitrogen to pyridine nitrogen is close to 1 : 1. Elemental analysis of the synthesized 2Cu-Co@N-MPC catalyst showed that the nitrogen content in the catalyst was 5.29%. It shows that N in 2Cu-Co@N-MPC is well introduced into the catalyst support and mainly exists in the form of graphitic nitrogen and pyridine nitrogen.

4.1.3. N_2 Desorption Analysis. The pore size distribution of the catalyst support and the internal structure of the pores have a great influence on the catalytic activity. By observing the N_2 isotherm adsorption and desorption curves (Figure 6), it can be seen that the prepared 2Cu-Co@N-MPC-500 has obvious pore structure characteristics, and the specific surface area of the catalyst calculated by the formula is 20.16 $m^2\,g^{-1}$. It can be seen from the pore size distribution curve that the pore size distribution of the mesoporous carbon spheres is uniform, and the average pore size is about 4.9 nm, which belongs to the mesoporous range.

4.1.4. TEM Analysis. Through the detailed observation of TEM, as shown in Figure 7, the prepared catalyst carrier has obvious spherical characteristics, and it can be seen that the N element is uniformly distributed, and the N element is well introduced into the catalyst carrier. The copper-cobalt nanoparticles were well-dispersed in the pore size of the mesoporous carbon spheres, and there was no obvious metal agglomeration phenomenon, indicating that the prepared nitrogen-containing mesoporous carbon carrier had a good dispersing effect on the metal copper-cobalt nanoparticles.

4.2. Catalyst Performance Test. Taking furfural hydrogenation to cyclopentanone as a model reaction, the catalytic hydrogenation performance of the catalyst 2Cu-Co@N-MPC-500 was investigated. The reaction temperature, reaction pressure, and reaction time conditions were optimized. Under the mild reaction conditions of 150°C, 2 MPa H_2, and 2 h, the 2Cu-Co@N-MPC-500 catalyst showed the best catalytic activity and selectivity. A furfural conversion of 96.1% and a cyclopentanone yield of 75.2% were obtained. Subsequently, the effect of nitrogen content in the carrier on the catalytic activity and the cyclic stability of the catalyst were investigated in depth.

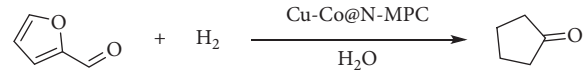

4.2.1. Effect of Nitrogen Content in the Catalyst Carrier on the Reaction Activity. The catalytic performance of catalysts with different nitrogen content in furfural hydrogenation was tested experimentally, and the results are shown in Figure 6. Using the traditional activated carbon-supported bimetallic catalyst 2Cu-Co@AC-500 under the optimal reaction conditions, 78% furfural conversion and 35% cyclopentanone yield can be obtained. However, the as-prepared N-doped catalyst 2Cu-Co@N-MPC-500 was able to achieve close to 100% conversion and 75% cyclopentanone yield under optimal reaction conditions, suggesting that the use of the N-doped mesoporous catalyst is beneficial. The carbon material as a carrier can effectively improve the activity of furfural hydrogenation and the selectivity to cyclopentanone. In order to better understand the role of N-doped support in the catalytic hydrogenation of furfural, the nitrogen content in the support was adjusted by changing the molar ratio of m-aminophenol to formaldehyde to test the addition of catalysts with different N contents in the support. Hydrogen activity, the results are shown in Figure 8. With the increase of N doping content from 2.46 % to 6.67 %, the furfural conversion showed a trend of increasing first and then tending to be stable, while the yield of cyclopentanone kept increasing. When the nitrogen doping in the carrier is 2.46 %, the furfural conversion and cyclopentanone yield are 86% and 59%, respectively. When the nitrogen doping in the carrier is increased to 5.92 %, the furfural conversion and cyclopentanone yield are 86% and 59%, respectively. The yields of ketones reached 95% and 75%, respectively, which indicated that proper N doping was very important to improve the hydrogenation activity and selectivity of furfural. For the type of N-doped support, the main forms of N in the catalyst support are pyridine nitrogen and graphitic nitrogen, and

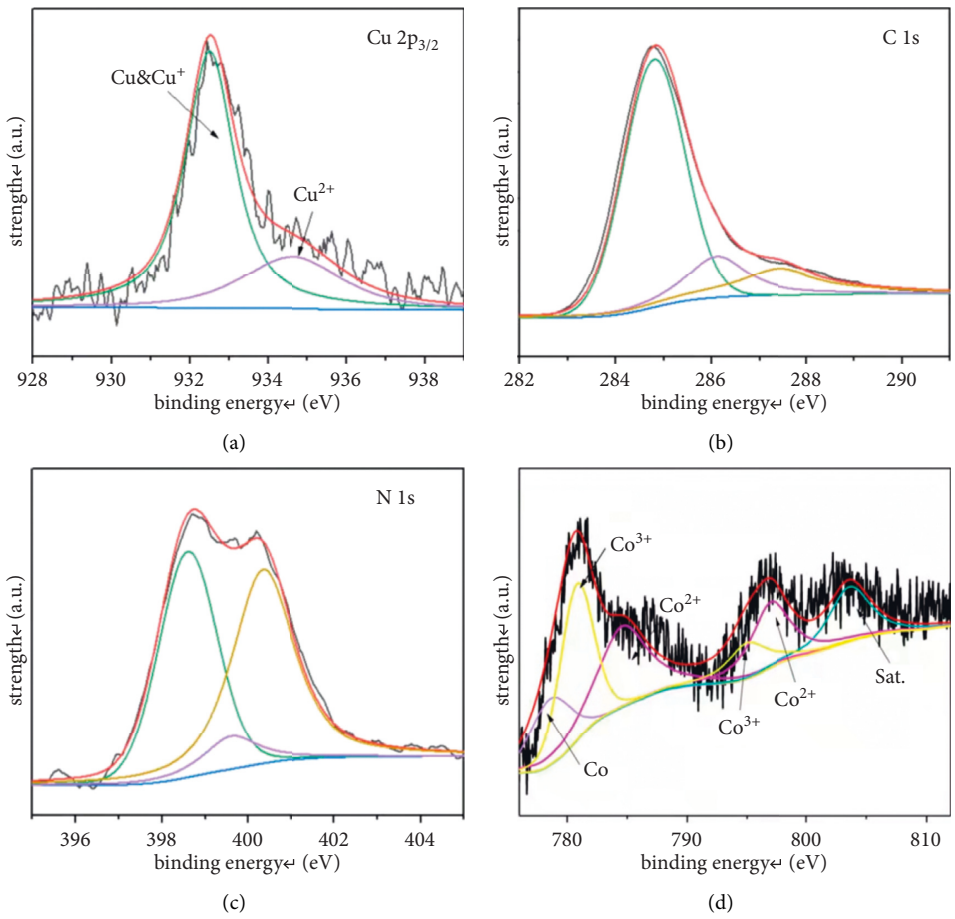

Figure 5: XPS characterization of 2Cu-Co@N-MPC-500.

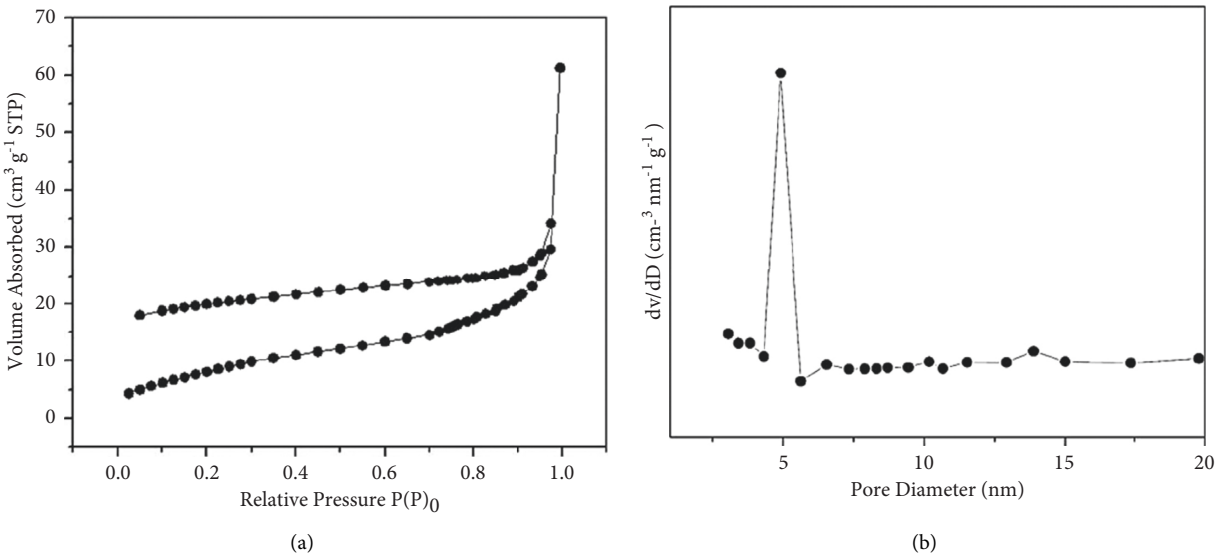

Figure 6: BET characterization of 2Cu-Co@N-MPC-500.

the presence of pyridine nitrogen and graphitic nitrogen plays a positive role in the hydrogenation of furfuryl alcohol to cyclopentanone. The summary includes the following reasons: (1) The introduction of nitrogen into the catalyst can provide an anchor for the nanometal particle components, form metal-N bonds, enhance the interaction between

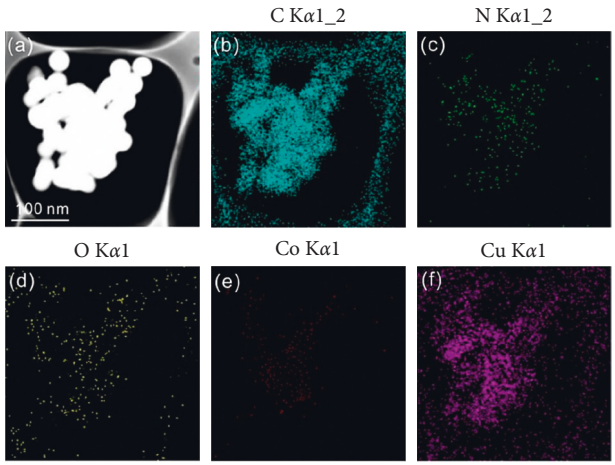

Figure 7: TEM and EDX characterization images of 2Cu-Co@N-MPC-500.

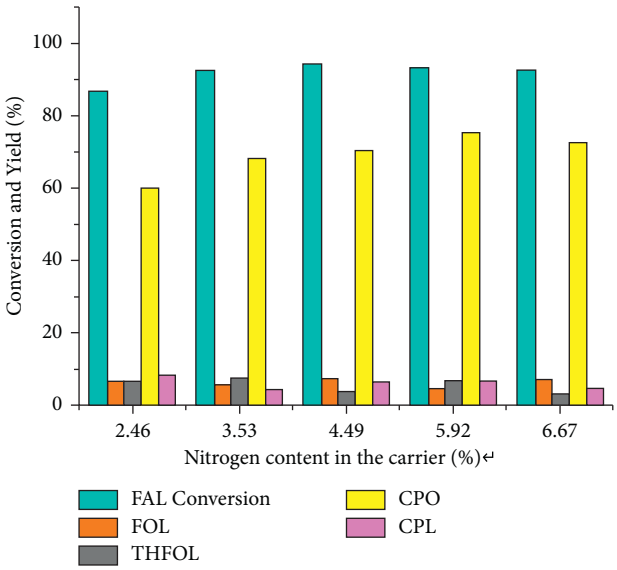

Figure 8: Effect of nitrogen content in the carrier on the catalytic activity.

the metal active components and the support, and effectively regulate the metal activity. The size and dispersion of the components make it difficult for the metal particle components to agglomerate; (2) the pyridine nitrogen present in the catalyst carrier can increase the Lewis basic site and enhance the adsorption effect on the reactants; (3) the introduction of N in the carrier doping can effectively improve the electron transfer rate and increase the electron density of the catalyst metal particles, thereby increasing the interaction between it and the reactant furfural [12–18]; (4) the introduction of nitrogen in the carrier can effectively increase the catalyst's efficiency. Hydrophilic, there is a ring-opening process in the hydrogenation of furfural to cyclopentanone, and water plays an indispensable role in the ring-opening process, which has an important impact on improving the reactivity and selectivity.

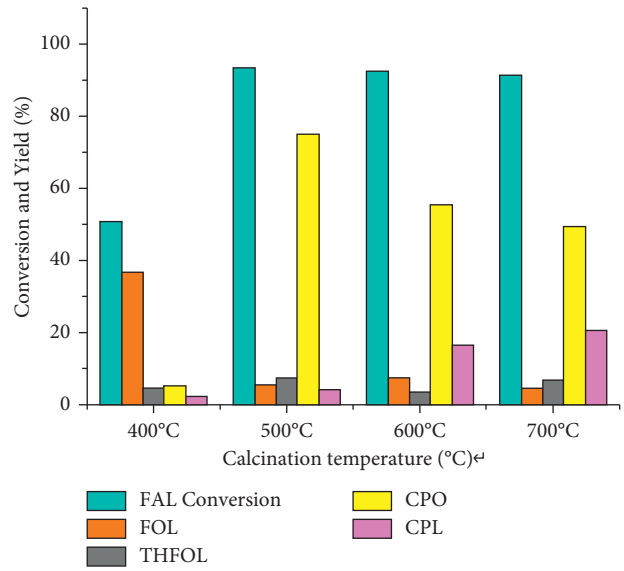

Figure 9: Catalyst cycle performance diagram.

4.2.2. Catalyst Cycle Performance Test. The 2Cu-Co@N-MPC-500 catalyst was subjected to cycling experiments, and the specific experimental results are shown in Figure 9. The experimental results show that the yield of cyclopentanone is only slightly decreased after the catalyst is recycled for 5 times, and the furfural is basically completely converted. The furfural conversion and cyclopentanone yields can still reach 90% and 71%, respectively, in the fifth cycle.

Through ICP-AES analysis, it was found that the Cu and Cu contents in the initial catalyst were 3.48% and 1.62%, respectively. After 5 cycle experiments, the metal contents of Cu and Co in the catalyst were 3.22% and 1.35%, respectively, and only a small part of the active metal was lost in the cycle reaction. The 2Cu-Co@N-MPC-500 catalyst was used in furfural hydrogenation. It exhibits good reusability and high stability in the selective formation of cyclopentanone. The excellent stability is attributed to the carbon support that can well immobilize and protect the bimetallic nanoparticles, while the doping of nitrogen forms metal-N bonds, which increases the interaction between the support and the bimetallic Cu-Co [19, 20].

5. Conclusion

In this paper, based on the preparation of nitrogen-doped carbon-based bimetallic copper-cobalt catalysis and its monitoring application in furfural hydrogenation, by using m-aminophenol as the nitrogen source, formaldehyde as the carbon source, and P123 as the template agent, a nitrogen-doped carbon-based metal catalyst 2Cu-Co@N-MPC-500 was hydrothermally synthesized and characterized by XRD, XPS, BET, and TEM. The catalyst was analyzed, and the results showed that the catalyst had a stable carbon sphere structure, uniform pore size distribution, and uniform dispersion of metal nanoparticles. It exhibits excellent selectivity and cycle stability in the hydrogenation of furfural to cyclopentanone. Under the optimal conditions, the conversion rate of furfural reached 96.1%, the yield of

cyclopentanone reached 76.2%, and the catalyst was cycled 5 times without obvious deactivation.

Data Availability

The dataset can be accessed upon request.

Conflicts of Interest

The authors declare that there are no conflicts of interest.

Acknowledgments

This study was supported by General project of National Natural Science Foundation of China: design and preparation of the GPH-(CH2) n-bm catalyst with flexible "bridge chain" and research on "quasi-homogeneous" catalytic performance (21971050); 2020.1 ~ 2023.12, and Key project of Natural Science Research Project of Colleges and Universities in Anhui Province (No. kj2019a1248).

References

[1] S. Wang, Q. Zhao, H. Wei et al., "Aggregation-free gold nanoparticles in ordered mesoporous carbons: toward highly active and stable heterogeneous catalysts," *Journal of the American Chemical Society*, vol. 135, no. 32, pp. 11849–11860, 2013.

[2] Y. Tian, P. Liu, X. Wang, and H. Lin, "Adsorption of malachite green from aqueous solutions onto ordered mesoporous carbons," *Chemical Engineering Journal*, vol. 171, no. 3, pp. 1263–1269, 2011.

[3] D. Wang, A. Fu, H. Li et al., "Mesoporous carbon spheres with controlled porosity for high-performance lithium-sulfur batteries," *Journal of Power Sources*, vol. 285, pp. 469–477, 2015.

[4] S. Kasakov, C. Zhao, E. Baráth et al., "Glucose- and cellulose-derived Ni/C-SO3H catalysts for liquid phase phenol hydrodeoxygenation," *Chemistry - A European Journal*, vol. 21, no. 4, pp. 1567–1577, 2015.

[5] A. Onda, T. Ochi, and K. Yanagisawa, "New direct production of gluconic acid from polysaccharides using a bifunctional catalyst in hot water," *Catalysis Communications*, vol. 12, no. 6, pp. 421–425, 2011.

[6] H. Jiang, X. Yu, R. Nie, X. Lu, D. Zhou, and Q. Xia, "Selective hydrogenation of aromatic carboxylic acids over basic N-doped mesoporous carbon supported palladium catalysts," *Applied Catalysis A: General*, vol. 520, pp. 73–81, 2016.

[7] K. A. Kurak and A. B. Anderson, "Nitrogen-treated graphite and oxygen electroreduction on pyridinic edge sites," *Journal of Physical Chemistry C*, vol. 113, no. 16, pp. 6730–6734, 2009.

[8] Z. Lei, L. An, L. Dang et al., "Highly dispersed platinum supported on nitrogen-containing ordered mesoporous carbon for methanol electrochemical oxidation," *Microporous and Mesoporous Materials*, vol. 119, no. 1-3, pp. 30–38, 2009.

[9] C. E. Chan-Thaw, A. Villa, G. M. Veith et al., "Influence of periodic nitrogen functionality on the selective oxidation of alcohols," *Chemistry - An Asian Journal*, vol. 7, no. 2, pp. 387–393, 2012.

[10] S. C. Petitto and M. A. Langell, "Cu2O(110) formation on Co3O4(110) induced by copper impurity segregation," *Surface Science*, vol. 599, no. 1-3, pp. 27–40, 2005.

[11] H. Sohn, I. I. Soykal, S. Zhang et al., "Effect of cobalt on reduction characteristics of ceria under ethanol steam reforming conditions: AP-XPS and XANES studies," *Journal of Physical Chemistry C*, vol. 120, no. 27, pp. 14631–14642, 2016.

[12] D. Guo, R. Shibuya, C. Akiba, S. Saji, T. Kondo, and J. Nakamura, "Active sites of nitrogen-doped carbon materials for oxygen reduction reaction clarified using model catalysts," *Science*, vol. 351, no. 6271, pp. 361–365, 2016.

[13] Z. Li and J. Chen, "Prognostics of PEM fuel cells based on Gaussian process state space," *Journal of Energy*, vol. 149, pp. 63–73, 2018.

[14] Z. Hu, L. Xu, J. Li et al., "A novel diagnostic methodology for fuel cell stack health: performance, consistency and uniformity," *Energy Conversion and Management*, vol. 185, pp. 611–621, 2019.

[15] H. Lu, J. Chen, C. Yan, and H. Liu, "On-line fault diagnosis for proton exchange membrane fuel cells based on a fast electrochemical impedance spectroscopy measurement," *Journal of Power Sources*, vol. 430, pp. 233–243, 2019.

[16] N. H. Behling, *Fuel Cells: Current Technology Challenges and Future Research Needs*, Elsevier Science, Hefei, China, 2012.

[17] D. M. Du-Plooy and J. Meyer, "PEM fuel cells: failure, mitigation and dormancy recoveryunderstanding the factors affecting the efficient control of PEMFC [C]," *IEEE Africon*, vol. 2017, no. 9, pp. 1119–1124, 2017.

[18] J. Chen, D. Zhou, C. Lyu, and C. Lu, "A novel health indicator for PEMFC state of health estimation and remaining useful life prediction," *International Journal of Hydrogen Energy*, vol. 42, no. 31, pp. 20230–20238, 2017.

[19] D. Zhang, P. Baraldi, C. Cadet, N. Yousfi-Steiner, C. Bérenguer, and E. Zio, "An ensemble of models for integrating dependent sources of information for the prognosis of the remaining useful life of Proton Exchange Membrane Fuel Cells," *Mechanical Systems and Signal Processing*, vol. 124, pp. 479–501, 2019.

[20] Y. Hou, Z. Yang, and G. Wan, "An improved dynamic voltage model of PEM fuel cell stack," *International Journal of Hydrogen Energy*, vol. 35, no. 20, pp. 11154–11160, 2010.